Simulations of length-scale change for finger growth in intercalation compounds

G. R. Carlow* and R. F. Frindt
Department of Physics, Simon Fraser University, Burnaby, British Columbia, Canada V5A 1S6
(Received 2 May 1994)

The dynamics of domain growth in intercalation compounds has been investigated using computer simulations. The system has been modeled as sheets of two-dimensional diffusive lattice gas with attractive interactions within the sheets and repulsive interactions between atoms in adjacent sheets. The atoms enter the "crystal" from a reservoir at one edge. For a stage-2 phase with alternate-layer occupancy the results show a fingerlike domain formation which propagates in from the crystal edge. As fingers propagate into the crystal, the length scale increases via a merging mechanism. Finger formation and merging is also seen during simulations of deintercalation of a filled crystal. The results are in qualitative agreement with stage-2 intercalation domains reported previously in Ag-intercalated TiS_2.

I. INTRODUCTION

Intercalation of a layered material involves the introduction of foreign atoms, or molecules, into the regions between the layers. The process involves two-dimensional (2D) motion of the intercalant since diffusion through the layers is, in general, negligible.[1,3] Intercalation is frequently accompanied by a staging phenomenon,[3] where sheets of the intercalant are ordered perpendicular to the layers. The stage index n is used to designate the number of host layers between two intercalant sheets. There has been a great deal of evidence that staging occurs, not with continuous intercalant layers, but by the formation of domains[4,5] where within each domain the intercalant layers are not continuous but form islands, and, together with the host layers, form a staged structure. A regularization of this model, known as the Daumas-Hérold (DH) domain model,[6] is shown in Fig. 1 for a stage-2 structure. Domain models are particularly useful for explaining stage transformations in which the stage index changes.[7]

The lateral size and shape of islands and domains is recognized as being of crucial importance for the understanding of intercalation kinetics and stage transformations.[8] Typical reported sizes are in the 100–10 000-Å range for graphite intercalation compounds.[4,7,9,10] Recently, Auger microscopy of the surfaces of cleaved, stage-2 partially intercalated Ag/TiS_2 single crystals revealed real-space pictures of intercalant islands.[11] The lateral shape of the islands were in the form of narrow fingerlike structures, or "channels," which extended from the intercalated crystal edge to the intercalation front—a distance ranging from 100 to 200 μm. The width of the channels was about 5 μm and the in-plane periodicity was about 10 μm. Such channel structures were also seen in Ag/TiS_2 systems deintercalated from stage 1 to stage 2. These results provide evidence for a regular domain structure. However, how such channels form and grow is not known, mainly due to the lack of experimental techniques which have both the spatial and time resolution required. In addition, what determines the channel length scale of 10 μm remains unanswered

In recent years, full three-dimensional Monte Carlo simulations of intercalation have been carried out. The results of Kirczenow's[12] simulated graphite intercalation compounds showed real-space pictures which revealed staging, domain structure, stage transitions, and stage disorder. More recently, Weber and Butz[13] simulated lithium intercalation in TaS_2 and observed density domains, superlattice ordering, and front velocities that were in agreement with experiment and, under certain parameter conditions, reported that fingerlike structures could be obtained.

Current theory attributes domain formation to elastic and electrostatic interactions. Elastic effects result when guest atoms enter the host material and the host layers locally deform in order to accommodate the guest. The configuration of the guest atoms will be such as to minimize the bending energy of the host. Theory by Safran and Hamman[14] treated the host as an anisotropic elastic continuum deformed by the guest atoms. Their result was that the effective elastic interaction between guest atoms within a given gallery between two host layers was attractive and encouraged island formation, and that the interaction of guest atoms separated by a c-axis displacement, was repulsive. This creates a tendency for islands formed in neighboring galleries to be "staggered" along the c axis, giving rise to domains. Electrostatic effects arise from charge transfer between the guest and the host. The Coulomb repulsion between charged intercalant layers, or islands, also favors staggered islands along the c axis.

In this paper we present a study of Monte Carlo simulations of intercalation and deintercalation. The simula-

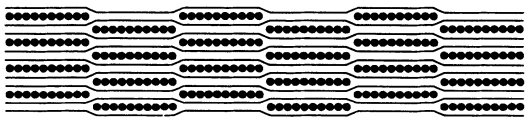

FIG. 1. A schematic of a stage-2 Daumas Hérold domain structure showing six domains. The lines represent the host layers and the circles represent the intercalant. The elastic deformation of the host layers is shown schematically.

0163-1829/94/50(15)/11107(9)/$06.00

tions are based on a model for Ag-intercalated TiS_2. We report on the formation of fingerlike structures and show a mechanism responsible for increasing the length scale of such structures.

II. THE MODEL

The galleries of $1T$-TiS_2 crystals have two types of available sites for intercalated atoms to occupy, namely sites that are octahedrally and tetrahedrally coordinated by sulfur atoms. Within a gallery there is one octahedral and two tetrahedral sites per Ti atom and the octahedral sites form a triangular lattice. From x-ray diffraction, it is known that Ag atoms intercalated into the galleries of TiS_2 reside in the octahedral sites.[15] The a_0 and the c_0 spacings of the octahedral sites in an unintercalated crystal are 3.407 and 5.696 Å, respectively.[16] This information is used to construct a "crystal" for the simulations. The crystal consists of a three-dimensional array of allowed sites, of size N_x by N_y by N_z, which intercalant atoms can occupy. The xy planes, representing galleries of octahedral sites, each form a 2D triangular lattice. The other possible sites for Ag, the tetrahedral sites, are ignored. The intercalant enters the crystal from a reservoir at the $y=1$ edge and, once inside, can move in the xy plane only. This type of movement reflects the observation that Ag does not diffuse through TiS_2 layers.[2] Periodic boundary conditions are used in both the x and z directions and the $y=N_y$ edge can be left free, so that particles can leave the crystal at that edge, or it can be left clamped. The $y=N_y$, or far edge, boundary condition becomes important when attempting to model an infinite crystal. The clamped edge models a finite system, whereas the unclamped edge does not allow an intercalant that has diffused beyond the far edge to return.

The particles of the intercalant in the simulations represent individual atoms of Ag, in contrast to the elementary islands of the intercalant used by Kirczenow.[12] At most one atom can occupy a lattice site.

Intercalant atoms enter and leave the crystal via the reservoir. The reservoir is treated as with Kirczenow:[12] at any given time, a reservoir site is occupied by an intercalant atom with a probability given by

$$P_{rs}=\frac{e^{-(E_{rs}-\mu_R)/kT}}{1+e^{-(E_{rs}-\mu_R)/kT}}\ , \tag{1}$$

where E_{rs} is the energy of the intercalant in the reservoir, μ_R is the chemical potential of the reservoir, k is Boltzmann's constant, and T is the temperature. E_{rs} can be thought of as an adsorption energy of the intercalant species onto the crystal surface.[12]

The model Hamiltonian used for the intercalant in the crystal is

$$H=\sum V_{\rm el}(r,z)+\sum V_{\rm est}(r,z)\ , \tag{2}$$

where $V_{\rm el}(r,z)$ and $V_{\rm est}(r,z)$ are the elastic and electrostatic interactions, respectively, for two atoms separated by an in-plane distance r and an out-of-plane distance z. The sums are carried out over all intercalant atoms in the crystal.

The elastic interaction is treated in the Safran-Hamman model,[14] which provides an attractive intralayer interaction and a repulsive interlayer interaction. In the model, the interaction energy between two spatially separated elastic dipoles is

$$V_{\rm el}(r,z)=\frac{-P^2(a_3r^2-2z^2)}{4\pi C_{44}(a_3r^2+z^2)^{5/2}}\ , \tag{3}$$

where $a_3=C_{33}/C_{44}$, C_{33}, and C_{44} are the elastic constants of the host material, P is the elastic dipole strength of an intercalated atom, r is the in-plane separation of the dipoles, and z is the c-axis separation of the dipoles. Note that this elastic model deals with particle-particle interactions only, thereby neglecting effects associated with three or more particles. Also note that we ignore the long-range elastic strain that results in U-shaped intercalation fronts along the c axis of partially intercalated crystals.[17] We assume that our simulations predict behavior near the middle of a crystal along the c axis, where, due to symmetry, we do not expect this strain to affect our results.

The electrostatic interactions arise because of charge transfer between the guest and the host upon intercalation. The electrostatic interactions between charged intercalate atoms is always repulsive, and can be estimated from the change in the open circuit potential versus the Ag fraction x for Ag_xTiS_2.

As can be seen, the parameter list is quite formidable, containing P, C_{33}, C_{44}, $V_{\rm est}(r,z)$, E_{rs}, μ_R, and T. In order to estimate their values, the following assumptions will be made: (i) As mentioned above, only the octahedral sites are considered. (ii) Since only stages 1 and 2 have been observed in Ag-TiS_2, the out-of-plane interactions are most likely "short-range" (as compared to, say, graphite, where many high stages have been observed). Therefore, only nearest-neighbor (NN) out-of-plane interactions are considered. However, since TiS_2 layers are quite rigid,[18] the in-plane elastic interactions are considered "long-range" and will include up to the fourth NN. (iii) At a temperature of about 250 K the Ag-occupied regions, in both stage-1 and stage-2 phases, form a $\sqrt{3}a$ by $\sqrt{3}a$ superlattice.[19] This geometry will be used for an estimation of $V_{\rm est}$. (iv) It is assumed that the in-plane electrostatic interactions are strongly screened by the host layers, so only NN in-plane electrostatic interactions are included.

The model parameters are now estimated using these assumptions along with the following experimental data.

(a) The elastic constants were determined from phonon-dispersion curves from neutron-scattering experiments on TiS_2 crystals.[20] The approximate values are $C_{33}\approx 55\times 10^9$ N/m^2 and $C_{44}\approx 18\times 10^9$ N/m^2.

(b) The value for P for lithium (in graphite) has been estimated at 3.3 eV.[21] P is proportional to the increase in volume of the host upon intercalation,[22] and since the change in a spacing is negligible, we assume that P is proportional to δc, where δc is the change in c spacing. Using $P_{\rm Li}\approx 3.3$ eV and $\delta c_{\rm Li}\approx 0.4$ Å for $Li_{0.4}TiS_2$,[23] and $\delta c_{\rm Ag}\approx 0.75$ Å for $Ag_{0.4}TiS_2$, gives the result $P_{\rm Ag}\approx 6$ eV.

(c) In order to estimate the electrostatic parameters, we turn to the open circuit potential $V(x)$ versus Ag fraction

x curve for the Ag-TiS_2 cell.[24] From these curves at $x=0.33$ an "ideal" stage 1 exists, and between $x\approx 0.33$ and 0.4 there is a sudden drop in the curve of about 0.045 V. Assuming the existence of an ordered Ag triangular superlattice at $x=0.33$, this potential difference, corresponding to an energy difference of 0.045 eV (the energy required to intercalate another atom), is approximately three times the NN in-plane interaction energy. So

$$3[V_{\rm el}(a_0,0)+V_{\rm est}(a_0,0)]=0.045 \text{ eV} .$$

Using the estimated parameters gives $V_{\rm el}(a_0,0)=-0.125$ eV, so that $V_{\rm est}(a_0,0)=0.14$ eV. To roughly estimate an out-of-plane electrostatic parameter, we again turn to the $V(x)$ curves. At $x=0.17$ an "ideal" stage 2 exists, and between $x\approx 0.17$ and 0.2 there is a drop in the curve in the 0.04–0.05-V range. As an approximation, this potential difference, corresponding to an energy difference of about 0.4–0.05 eV, is twice the NN out-of-plane interaction, multiplied by $\frac{1}{3}$ (since each NN out-of-plane site is occupied with $\frac{1}{3}$ probability due to the local Ag concentration). Therefore, using the 0.04-eV value,

$$\tfrac{2}{3}[V_{\rm el}(0,c_0)+V_{\rm est}(0,c_0)]=0.04 \text{ eV} , \quad (4)$$

so that a value of about 0.065 eV is obtained for the total (elastic and electrostatic) NN out-of-plane interaction.

We note that using $c_0=5.696$ Å and the estimated parameters in Eq. (4), we obtain $V_{\rm est}(0,c_0)\approx -0.22$ eV, where the negative sign corresponds to an attractive interaction between like charges. The inconsistency could be due to the continuum assumption of the Safran-Hamman model. This assumption may be realistic for the in-plane interactions, since TiS_2 layers are quite rigid, while it may not be for the out-of-plane interactions due to the weak van der Waals bonding of the layers.

(d) The reservoir energy E_{rs} is not known. For this reason it has been left as a free parameter.

(e) The chemical potential of the reservoir can be set as desired.

(f) The temperature is set to room temperature: 293 K.

This completes the parameter estimation. These parameter values merely represent a starting point for the simulations.

The Monte Carlo algorithm is now described. Lattice sites are given the value 1 if they are occupied and 0 if they are not, and no more than one particle can occupy a given site at one time. The reservoir sites are treated just like the lattice sites, except they do not have a definite occupancy. Instead, they have a value of 1 with the probability $P_{\rm rs}$, given by Eq. (1), and a value 0 with the probability $1-P_{rs}$. Starting from a configuration of the site occupancy, an occupied site is chosen at random along with, randomly, one of its six NN in-plane sites. (If, however, the initially chosen site is a reservoir site which turns out to be occupied, then one of its NN in-plane sites, of which there are only two, is chosen if a random number between 0 and 1 is less than $\frac{1}{3}$). If the NN site in the randomly chosen direction is occupied, then another occupied site is chosen at random, otherwise a trail move to this empty NN site is attempted. The change in energy, δE, of the system due to this attempted move is calculated from Eqs. (2), (3), and (4). If $\delta E<0$, then this attempted move is made, otherwise a random number between 0 and 1 is chosen. If this number is less than $\exp(-\delta E/kT)$ then the move is made, otherwise it is not. This process is then repeated. One Monte Carlo step (MCS) is defined as one trial move.

III. RESULTS

Initial simulations were done with the $y=N_y$ edge left free, or unclamped, so that particles could not be reflected from that edge. This boundary condition is meant to represent a crystal early in the intercalation process, where the intercalant concentration far from the reservoir remains quite low. After many simulations and an exploration of the effects of varying the parameters, we find that typical and interesting results are obtained with the following parameters: $C_{33}=55\times 10^9$ N/m^2, $C_{44}=18\times 10^9$ N/m^2, $P=5.25$ eV, $T=293$ K, $V_{\rm est}(a_0,0)=0.095$ eV, the total NN out-of-plane interaction at 0.045 eV, $\mu_R=0$, and $E_{rs}=0.025$ eV. The size of the crystal was set to $N_x=120$, $N_y=180$, and $N_z=4$ (four galleries).

The results of a simulation using these parameters are shown in Fig. 2. A dark spot indicates that a lattice site is occupied. For brevity only two neighboring galleries are shown. The reservoir is in contact with the top edge of each gallery and is not explicitly shown. The initial configuration was an empty crystal and columns (a)–(h) show the intercalant distributions in the crystal after 0.05, 0.1, 0.4, 0.7, 1, 2, 4, and 7 million Monte Carlo steps (MMCS), respectively. As can be seen in the figure, early in the intercalation process [columns (a) and (b)] each gallery starts to fill with the intercalant, and the average density of the intercalant in the vicinity of the reservoir is quite uniform. Locally, however, there are some high-density ($x=1$) regions. The high-density regions form due to the relatively strong, long-range in-plane elastic attraction. As intercalation progresses, the high-density regions extend farther into the crystal [columns (c), (d), and (e)]. These regions, which tend to be staggered from layer to layer due to the out-of-plane repulsive interaction, grow further into the crystal with time until a well-defined finger pattern emerges [column (h)]. The fingers form a stage-2 phase, with regions of stage 1 near the reservoir edge of the crystal. There are six fingers per gallery and the corresponding average wavelength, or length scale, is about 20 lattice spacings. For identical parameter sets, the number of fingers formed in each gallery varied between 6 and 7. The free edge or unclamped boundary condition had no effect on this finger formation since, by column (g), no intercalant had reached the far edge.

That the far-edge boundary condition is unimportant for relatively short simulation times was further confirmed by simulations using the identical parameter set with the far edge clamped where patterns essentially the same as those in Fig. 2 are observed.

Finger structures were obtained with many different parameter sets and were the only type of regular pattern observed. If fingers did form under a given set of conditions, results of simulations indicate that they would not

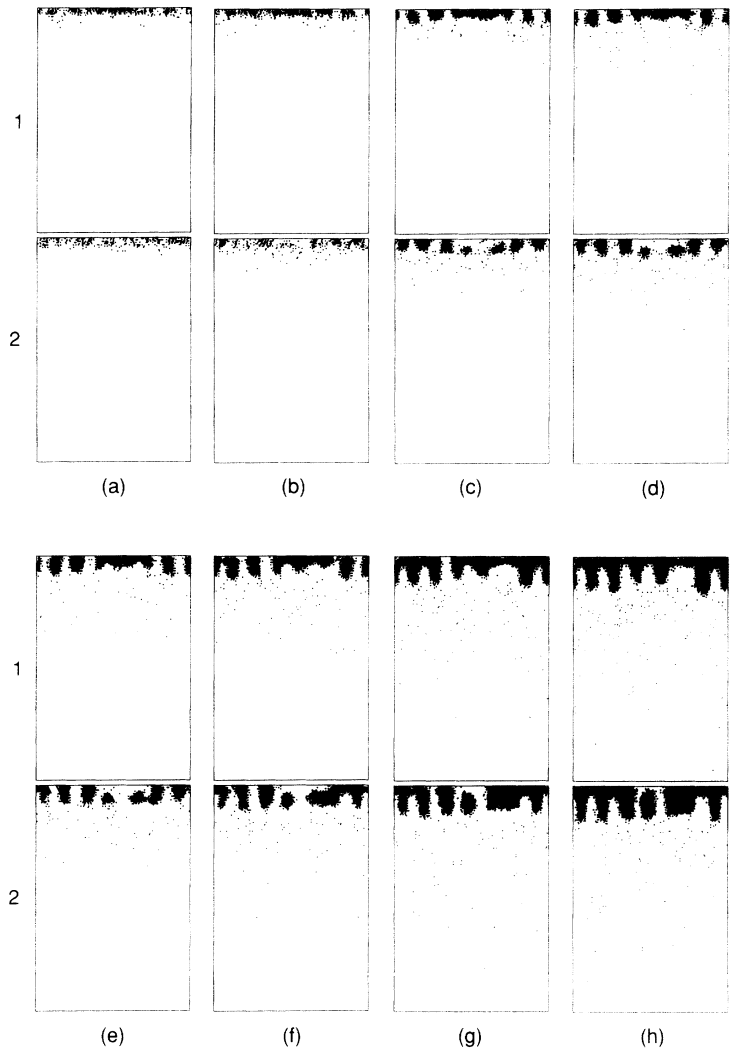

FIG. 2. Simulation showing finger formation early in the intercalation process. Each column shows two adjacent galleries (1 and 2) of the crystal. The simulation times are 0.05, 0.1, 0.4, 0.7, 1, 2, 4, and 7 MMCS for columns (a)–(h), respectively. The reservoir edge is at the top of each gallery, and the bottom edge is unclamped.

form if any one of the following was altered significantly: (1) the temperature was increased, (2) the reservoir chemical potential was decreased, (3) the in-plane elastic attraction was decreased, (4) the in-plane electrostatic repulsion was increased, or (5) the out-of-plane repulsion was decreased. The out-of-plane repulsion appears to be predominantly responsible for finger formation since, if its value was set to zero, no finger patterns were obtained for any combination of the remaining parameters tested. Figures 3–5 and 7 show simulations which demonstrate the effects of parameter variations.

The effects of temperature on finger formation are demonstrated in Fig. 3 where, except for temperature variations, the parameter set corresponds to that used in Fig. 2. It is seen that as the temperature increases the length scale tends to increase and the fingers gradually disappear.

Figure 4 demonstrates the dependence of finger formation on the interlayer repulsion energy, where it is seen that the length scale tends to increase with decreasing repulsion and, as expected, all structure disappears with zero interlayer repulsion. The parameter set in Fig. 4 corresponds to that in Fig. 2, except for the variation in the interlayer repulsion.

We have varied the elastic dipole strength P and the nearest-neighbor intralayer electrostatic repulsion in a systematic fashion in order to explore a small portion of the "phase diagram" of finger formation (although it

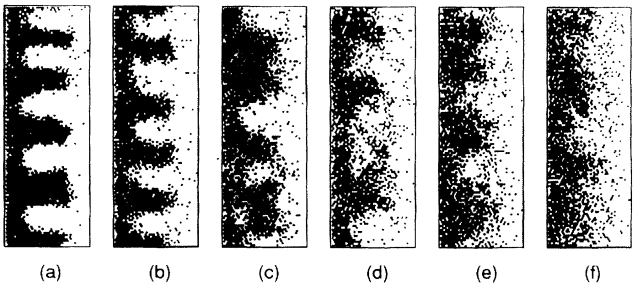

FIG. 3. Finger dependence of the temperature, showing a gallery of a crystal intercalated at different temperatures. The time for each simulation is 30 MMCS. The temperature is 293, 325, 425, 550, 650, and 700 K for columns (a) to (g), respectively. The reservoir is at the left of each gallery, and the right edge is unclamped. The lattice size is $N_x = 120$, $N_y = 40$, and $N_z = 6$.

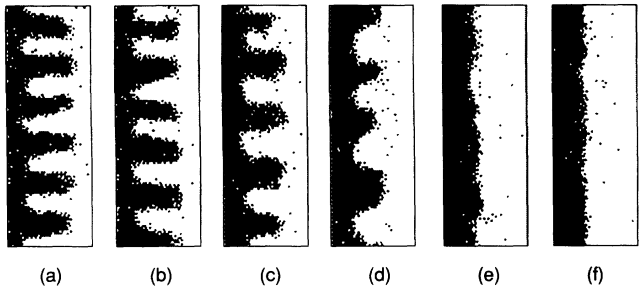

FIG. 4. Finger dependence of the interlayer interactions showing a gallery of a crystal intercalated with different interlayer repulsion energies. The time for each simulation was 30 MMCS. The interlayer repulsion energies are 0.045, 0.035, 0.025, 0.015, 0.005, and 0.0 eV for columns (a) to (f), respectively. The reservoir is at the left of each gallery, and the right edge is unclamped. The lattice size is $N_x=120$, $N_y=40$, and $N_z=6$.

must be kept in mind that we have nonequilibrium situations). The effects of varying the in-plane electrostatic repulsion $V_{\rm est}$ are demonstrated in Fig. 5, where for strong repulsion [Fig. 5(a)] a $\sqrt{3}a_0\times\sqrt{3}a_0$ ($x=\frac{1}{3}$) superlattice with no finger structure is obtained. With a decrease in the in-plane repulsion, higher-density ($x=1$) regions along with finger formation are observed. We have found in general that the transition from no fingers to fingers is very sensitive to the values of P and $V_{\rm est}$. For example, in Fig. 5, $V_{\rm est}$ changes by only 3% in going from (c) to (d). Figure 6 shows a plot of P vs $V_{\rm est}$ for a number of simulations. It is clear from Fig. 6 that as the in-plane repulsion is decreased, finger formation is favored as the effects of in-plane elastic attraction and the out-of-plane repulsion start to dominate. In Fig. 6 the data points were determined by visual inspection of the simulations. The uncertainty in $V_{\rm est}$ in determining the data points in Fig. 6 is about 0.002 eV.

For the simulation results presented thus far, the high-density ($x=1$) regions are involved in the finger formation. Since it is known that for Ag_xTiS_2 the occupied Ag density is about $x=0.4$, we have also simulated finger formation for densities less than $x=1$. To do this, starting from our basic parameter set, we changed the intralayer interactions to obtain the $x=\frac{1}{3}$ superlattice [similar to Fig. 5(a)] and then adjusted the interlayer repulsive interactions. We found that in order to obtain low-density fingers it was necessary to increase the range of the out-of-plane interactions from nearest-neighbor V_{o1} (one above the other), to include the second-nearest-neighbor interaction V_{o2}—that is, the interaction of sites separated by relative coordinates (a_0,c_0). Figure 7 illustrates finger formation for low densities using the same parameters as in Fig. 2, except that $V_{\rm est}(a_0,0)=0.3$ eV, $P=8$ eV, $V_{o1}=0.025$ eV, and $V_{o2}=0.008$ eV. It can be seen that finger formation is obtained with a $\sqrt{3}\times\sqrt{3}$ superlattice and that there is an increase in the finger length scale in going from (a) to (e). In (e), the finger separation corresponds to about 60 lattice spacings, or about 200 Å. Some $x=\frac{2}{3}$ regions are also seen near the crystal edge in Fig. 7. The increase in crystal size and number of neighbor interactions required for low-density finger formation very significantly increases computer time, so that low-density fingers have not been as extensively explored as the high-density situation.

It is interesting to note the lines of defects that occur early in the simulations near the reservoir edge, as can be seen in Figs. 7(a)–7(d). These defects are the result of there being three possible configurations of the $x=\frac{1}{3}$ superlattice. (These three configurations, when superimposed, would form an $x=1$ system.) If two different configurations meet, a line of defects, or a grain boundary, forms. The grain boundaries (which reside mainly in the stage-1 band near the reservoir edge) tend to disappear as simulation time increases.

Perhaps the most interesting result to come out of the simulations, apart from the finger formation itself, is the observation of length-scale changes as intercalation proceeds. This is clearly seen in Fig. 8, which is a continuation of Fig. 2. Figure 8, columns (a)–(h), show the crystal at 9, 10, 20, 30, 40, 70, 100, and 280 MMCS, respectively. By 9 MMCS [column (a)] the six fingers that initially formed have extended further into the crystal, and two of the fingers in the second gallery begin to "merge." This merging is accompanied by the recession of a finger in the first gallery due to the out-of-plane repulsion. The merging is completed by 40 MMCS [column (e)], at which time two other fingers begin to merge. This merging continues and is completed by 100 [column (g)] and 280 MMCS [column (h)] there are only four fingers per gallery—giving an average length scale of 30 lattice spacings. The fingers still form a stage-2 phase, with a band of stage 1 near the reservoir edge of the crystal.

The behavior of the fingers for the simulation where

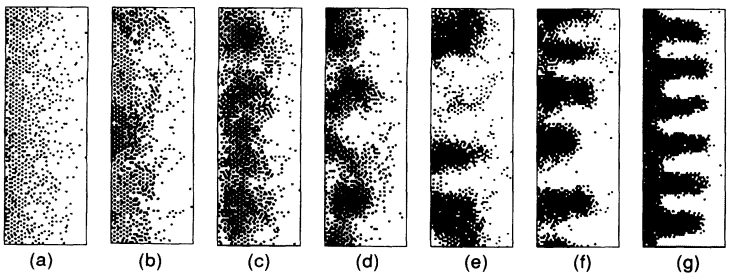

FIG. 5. Finger dependence on the in-plane repulsion showing a gallery of a crystal with different values of $V_{\rm est}$. The time for each simulation was 30 MMCS. $V_{\rm est}=0.1450$, 0.1120, 0.1100, 0.1095, 0.1080, 0.1050, and 0.0950 eV for columns (a) to (g), respectively. The reservoir is at the left of each gallery, and the right edge is unclamped. The lattice size is $N_x=120$, $N_y=40$, and $N_z=6$.

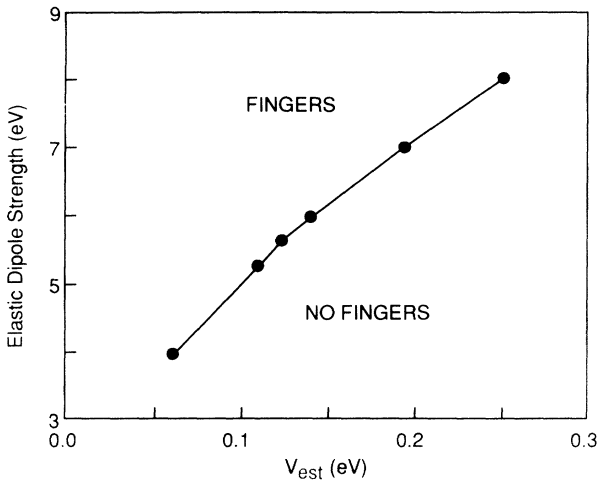

FIG. 6. A plot of the elastic dipole strength P, vs the in-plane electrostatic repulsion V_{est}, showing the transition region from finger to no finger formation. The remaining parameters are as in Fig. 5.

the far edge is clamped is very similar to the unclamped system. This is evident in Fig. 9 which is the latter part of a clamped system simulation. Columns (a)–(h) show the crystal at 20, 30, 40, 70, 100, 130, 230, and 480 MMCS, respectively. As the figure shows, merging continues in a similar manner as compared to the unclamped system, and by 480 MMCS [column (h)] there are four fingers per gallery—and the merging seen will soon result in only three fingers per gallery with an average length scale of about 40 lattice spacings.

Note that in Fig. 9, column (f), the first gallery contains a finger that has completely detached from the stage-1 band. This was found to be a common occurrence, but such isolated fingers were always seen to reattach, as indicated in column (g).

The "initial" length scale of the fingers, that is the first, well-defined length scale that appears in a simulation, was found to vary with the input parameters. The initial length scale could be made to increase by increasing the NN in-plane electrostatic repulsion, by decreasing the in-plane elastic attraction, by decreasing the reservoir energy, by increasing the temperature, or by decreasing the out of plane repulsion. The initial length scale was not changed by changing the size of the crystal in the x direction, or by changing the number of galleries in the crystal (the number of galleries was always an even number since an odd number of galleries combined with the periodic boundary conditions in the z direction would "frustrate" a stage-2 system).

We note that the finger length scale, or separation, is of the same order of magnitude as the finger length, and that the ratio of the finger length to the finger length scale tends to increase with simulation time, as in Fig. 8, columns (a) and (h), where its value increases from about 1 to about 2.5.

The simulations shown in Figs. 8 and 9 indicate that the far-edge boundary condition has little effect on finger formation and merging. However, what is affected by this boundary condition is the concentration x of the intercalant in the crystal as a function of the Monte Carlo time, t. At long t, for crystals with an unclamped far edge, particles leave the crystal in significant numbers, and it appears that x approaches a steady-state value between 0.35 and 0.4. Clamped systems intercalated for a sufficient length of time approached a complete stage-1, $x=1$ phase. In these systems, merging was seen to occur continually, and stopped only when the fingers reached the far edge of the crystal. In contrast, unclamped systems approaching a steady-state concentration showed little evidence of further merging.

Simulations of deintercalation were carried out by starting with a full crystal with $x=1$ and reducing the chemical potential of the reservoir to the point where the net concentration of the intercalant in the crystal decreased with Monte Carlo time. The parameter set used was the same as for Fig. 2 except that $\mu_R=-0.17$ eV and the lattice size was $N_x=120$, $N_y=120$, and $N_z=4$. The results are that deintercalation occurs via the formation of fingers in the stage-2 phase, and merging is also seen to occur. The merging mechanism during deintercalation is similar to that during intercalation if one views deintercalation as the intercalation of "holes" into a filled crystal.

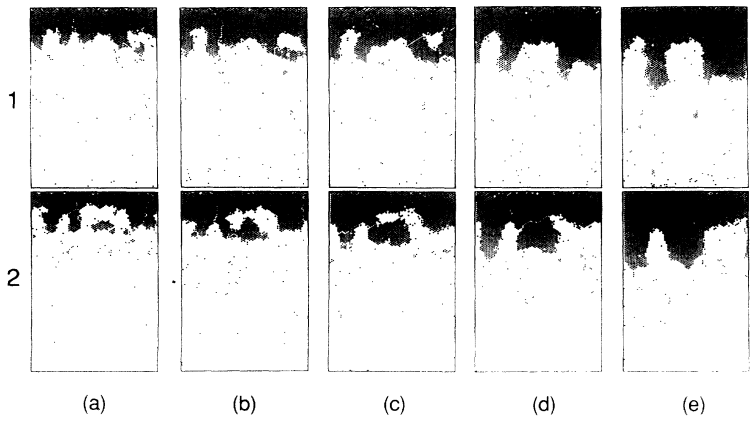

FIG. 7. Formation of intercalation fingers for low ($x=\frac{1}{3}$) atomic density for simulation times of 100, 200, 300, 500, and 1000 MMCS for columns (a) to (e), respectively. Each column shows two adjacent galleries (1 and 2) of the crystal. The reservoir is at the top of each gallery, and the bottom edge is clamped. $N_x=120$, $N_y=180$, and $N_z=4$.

IV. DISCUSSION

The simulations presented show real-space diagrams of intercalation, and the formation of fingerlike domains in a stage-2 model, and the length scale of the fingers as simulation time increases. While finger patterns appear to be stable, the separation of the fingers is not. The length scale initially depends on the input parameters, but increases with simulation time via an interesting merging mechanism. Finger patterns are formed and subsequent merging occurs in simulations where the far edge of the crystal is both clamped and unclamped. We believe it is reasonable to project that finger formation and merging will also occur in an infinite system, and that the finger length scale will continue to increase as intercalation continues.

We have shown that initial finger formation depends on elastic and electrostatic interactions of the intercalant in the crystal, as well as the chemical potential of the reservoir. We note that another parameter which may affect the initial formation of fingers is the geometry of active reservoir sites. Our simulations required the condition that all reservoir sites were active. If instead only a fraction of the sites were active, then initial finger formation could either be enhanced or hindered, depending on the relative positions of the active sites.

The increase of the length scale with simulation time can be understood in terms of energetics: the lowest-energy state for a stage-2 structure is a classically staged system, where the gallery occupancies alternate between completely empty and completely full. This configuration minimizes the domain-wall energy. However, at the beginning of intercalation, each gallery is equivalent, so that all galleries start to fill with the intercalant (or empty during deintercalation), and an initial finger pattern forms. The subsequent finger merging can therefore be thought of as a system attempting to reach a lower-energy state by reducing the domain-wall area.

For Ag-TiS_2 it is found that the ratio of the intercala-

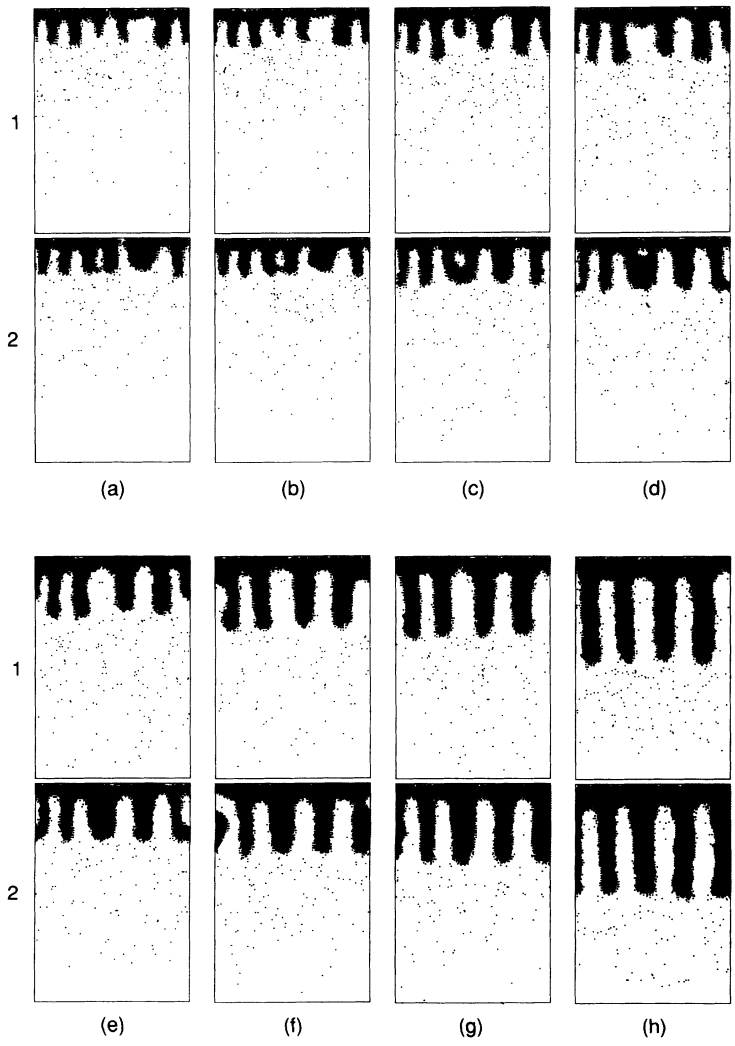

FIG. 8. Continuation of the simulation from Fig. 2 with the bottom edge unclamped for 9, 10, 20, 30, 40, 70, 100, and 280 MMCS for columns (a)–(h), respectively. Each column shows two adjacent galleries (1 and 2) of the crystal. Due to merging, the number of fingers decreases, and the widths of the fingers increases with simulation time.

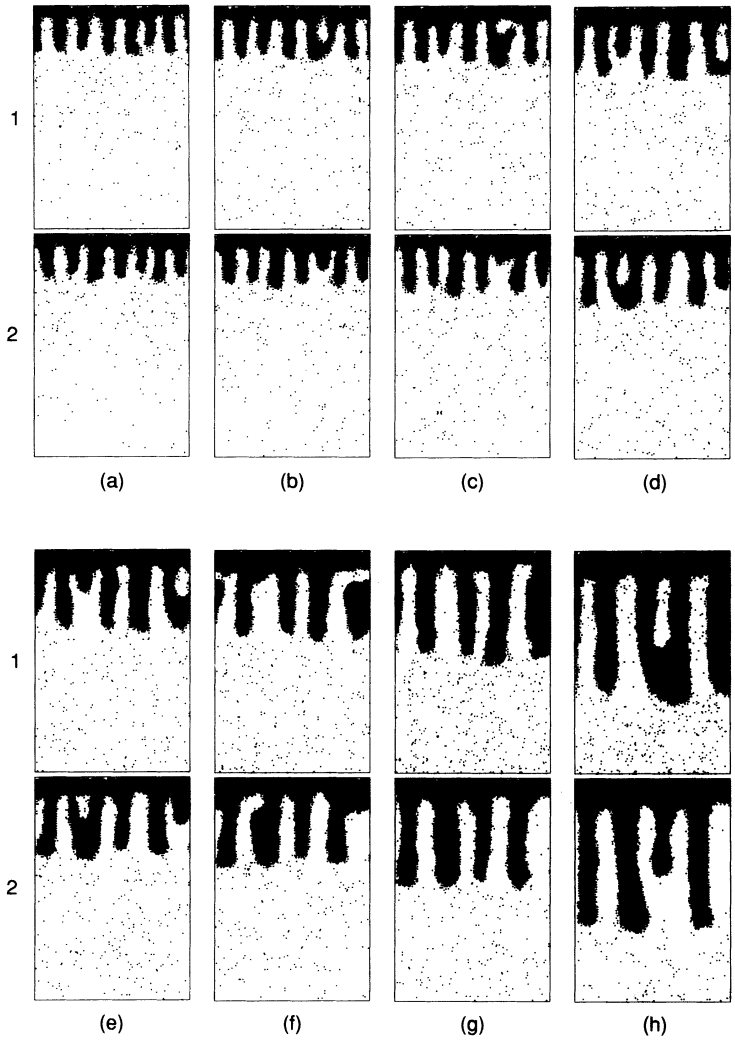

FIG. 9. A simulation with the bottom edge clamped showing four finger mergings for 20, 30, 40, 70, 100, 130, 230, and 480 MMCS for columns (a)–(h), respectively. Each column shows two adjacent galleries (1 and 2) of the crystal. The parameter set is the same as in Fig. 2.

tion distance to the finger separation is typically 10 to 1, or 20 to 1. For our simulations the ratio of the intercalation distance to the finger separation is typically around 1 at the initial appearance of fingers, and increases as intercalation proceeds. Thus we believe that simulations provide at least a good qualitative model for stage-2 intercalation and deintercalation.

ACKNOWLEDGMENTS

We thank D. Boal and G. Kirczenow for many helpful discussions. We also thank M. Weber and T. Butz for sending us helpful communications. This work was carried out with funding from the Natural Sciences and Engineering Council of Canada.

*Present address: Department of Physics, University of Western Ontario, London, Ontario, Canada N6A 3K7.

[1]J. G. Hooley, W. P. Garby, and J. Valentin, Carbon **3**, 7 (1965); J. G. Hooley, Mater. Sci. Eng. **31**, 119 (1977).

[2]D. Kaluarachchi and R. F. Frindt, Phys. Rev. B **31**, 3648 (1985).

[3]M. S. Dresselhaus and G. Dresselhaus, Adv. Phys. **30**, 139 (1981).

[4]M. E. Misenheimer and H. Zabel, Phys. Rev. B **27**, 1443 (1983).

[5]D. Kaluarachchi and R. F. Frindt, Phys. Rev. B **28**, 3663 (1983).

[6]N. Daumas and M. A. Hérold, C. R. Acad. Ser. C **268**, 373 (1963).

[7]R. Clarke, N. Wada, and S. A. Solin, Phys. Rev. Lett. **44**, 1616 (1980).

[8]S. A. Solin, in *Intercalation in Layered Materials,* Vol. 148 of *NATO Advanced Study Institute Series B: Physics,* edited by M. S. Dresselhaus (Plenum, New York, 1986), p. 173.

[9]J. M. Thomas, G. R. Millward, R. F. Schlögl, and H. P. Boehm, Mater. Res. Bull. **15**, 671 (1980).

[10]R. Levi-Setti, G. Crow, Y. L. Yang, N. W. Parker, R. Mittleman, and D. M. Hwang, Phys. Rev. Lett. **54**, 2615 (1985).

[11]G. R. Carlow, P. Joensen, and R. F. Frindt, Synth. Met. **34**, 623 (1989); G. R. Carlow, P. Joensen, and R. F. Frindt, Phys. Rev. B **42**, 1124 (1990).

[12]G. Kirczenow, Phys. Rev. Lett. **55**, 2810 (1985); G. Kirczenow, Can. J. Phys. **66**, 39 (1988).

[13]M. Weber and T. Butz, Phys. Rev. Lett. **66**, 361 (1991); M.

Weber (private communication).
[14]S. A. Safran and D. R. Hamann, Phys. Rev. Lett. **42**, 1410 (1979).
[15]G. A. Scholz and R. F. Frindt, Mater. Res. Bull. **15**, 1703 (1980).
[16]R. R. Chianelli, J. C. Scanlon, and A. H. Thompson, Mater. Res. Bull. **10**, 1379 (1975).
[17]D. Kaluarachchi and R. F. Frindt, Phys. Rev. B **39**, 8175 (1989).
[18]S. Lee, H. Miyazaki, S. D. Mahanti, and S. A. Solin, Phys. Rev. Lett. **62**, 3066 (1989).
[19]A. G. Gerards, H. Roede, R. J. Haange, B. A. Boukamp, and G. A. Wiegers, Synth. Met. **10**, 51 (1984/85); M. Mori, K. I. Oshima, S. C. Moss, R. F. Frindt, M. Plischke, and J. C. Irwin, Solid State Commun. **43**, 781 (1982); K. I. Oshima and S. C. Moss, Acta Crystallogr. A **39**, 298 (1983); R. M. Suter, M. W. Schafer, P. M. Horn, and P. Dimon, Phys. Rev. B **26**, 1495 (1982).
[20]M. Scharli and F. Levy, Phys. Rev. B **33**, 4317 (1986).
[21]H. Wagner, in *Hydrogen in Metals,* edited by G. Alefeld and J. Volkl (Springer, Berlin, 1978), Vol. I, p. 5.
[22]H. Wagner and H. Horner, Adv. Phys. **23**, 587 (1974).
[23]J. R. Dahn, W. R. McKinnon, R. R. Haering, W. J. L. Buyers, and B. M. Powell, Can. J. Phys. **58**, 207 (1980).
[24]G. A. Scholz and R. F. Frindt, J. Electrochem. Soc. **131**, 1763 (1984); J. Schramke and R. Schöllhorn, Solid State Ionics **23**, 197 (1987).

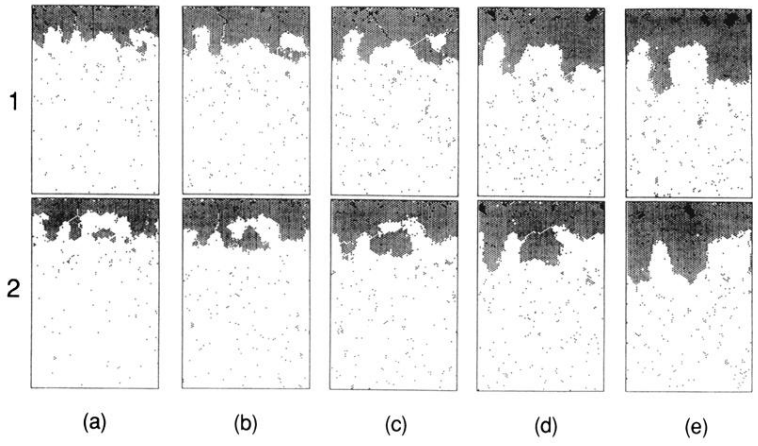

FIG. 7. Formation of intercalation fingers for low ($x = \frac{1}{3}$) atomic density for simulation times of 100, 200, 300, 500, and 1000 MMCS for columns (a) to (e), respectively. Each column shows two adjacent galleries (1 and 2) of the crystal. The reservoir is at the top of each gallery, and the bottom edge is clamped. $N_x = 120$, $N_y = 180$, and $N_z = 4$.

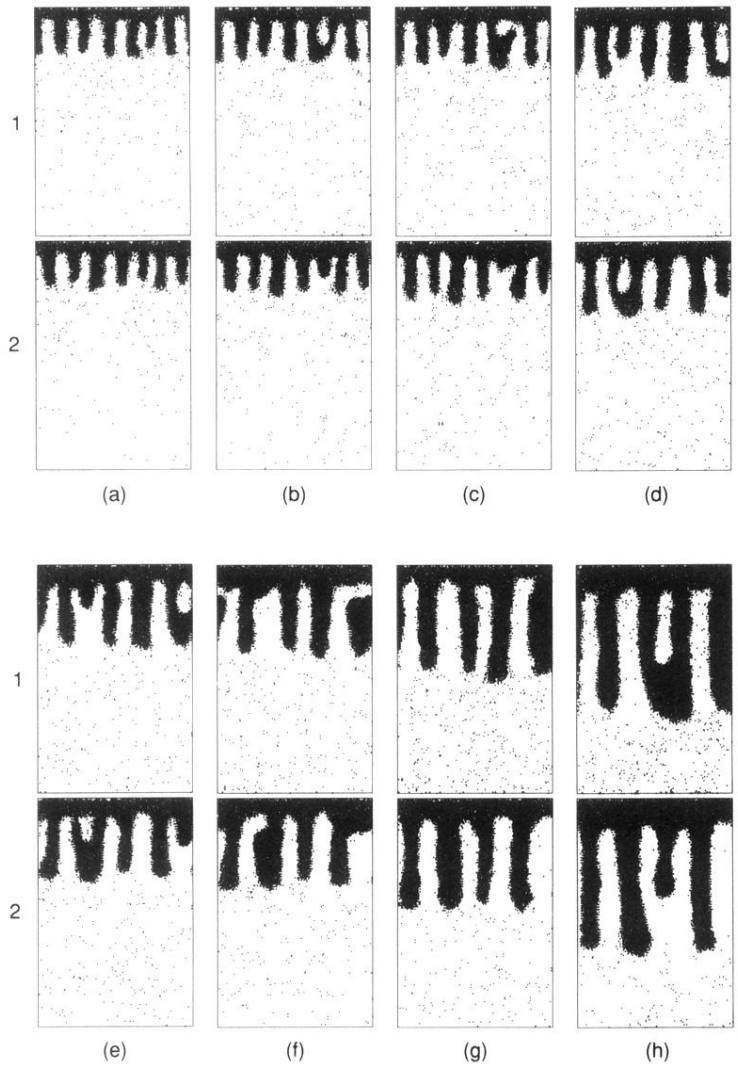

FIG. 9. A simulation with the bottom edge clamped showing four finger mergings for 20, 30, 40, 70, 100, 130, 230, and 480 MMCS for columns (a)–(h), respectively. Each column shows two adjacent galleries (1 and 2) of the crystal. The parameter set is the same as in Fig. 2.